Desalination and Water Treatment
www.deswater.com

doi: 10.1080/19443994.2015.1074122

57 (2016) 15276–15284
July

Taylor & Francis
Taylor & Francis Group

Study on the heat and mass transfer in AGMD module with latent heat recovery

Hongxin Geng[a,b,c], Long Lin[a,b,c], Pingli Li[a,b,c,*], Chunyao Zhang[a,b,c], Heying Chang[a,b,c]

[a]*School of Chemical Engineering and Technology, Tianjin University, Tianjin 300072, P.R. China, Tel. +86 022 27405902; Fax: +86 022 27404347; emails: genghongxin2008@126.com (H. Geng), linlong@tju.edu.cn (L. Lin), tdlpl@163.com (P. Li), zcy_878811325@126.com (C. Zhang), changheying@tju.edu.cn (H. Chang)*

[b]*Collaborative Innovation Center of Chemical Science and Engineering (Tianjin), Tianjin University, Tianjin 300072, P.R. China*

[c]*Tianjin Key Laboratory of Membrane Science and Desalination Technology, Tianjin University, Tianjin 300072, P.R. China*

Received 2 April 2015; Accepted 8 July 2015

ABSTRACT

A novel air gap membrane distillation (AGMD) module for desalination with latent heat recovery which consisted of parallel hollow fiber membranes and heat exchange hollow fibers was successfully developed. The temperature profiles of AGMD module designed with latent heat recovery along the radial direction and mass transfer coefficient across membrane (C_m), Knudsen diffusion coefficient across membrane (C_{Km}), molecular diffusion coefficient across membrane (C_{Mm}), and molecular diffusion coefficient in air gap (C_{Ma}) were obtained by establishing a heat and mass transfer model. The permeate flux (J_D) was highly sensitive to the hot feed inlet temperature, T_{hi}. The maximum value of J_D could reach 15.5 kg/m^2 h for module 1 and 20.2 kg/m^2 h for module 2 at T_{hi} = 90°C and T_{ci} = 30°C. The value of actual mass transfer coefficient across the membrane was in close to the value of Knudsen diffusion coefficient across the membrane, especially at high hot feed brine temperature. The membrane wall was the main resistance for mass transfer and contributed 60–70% to the total mass transfer resistance. The heat transfer across the heat exchange hollow fiber was the main heat transfer resistance and the heat transfer across the heat exchange hollow fibers was only around 3,238.1 W/m^2°C. The temperature polarization coefficient was introduced to measure the actual driving force.

Keywords: AGMD module; Latent heat recovery; Mass transfer; Heat transfer

1. Introduction

Water shortage is one of the most serious global challenges due to the exploding global population, rapid industrialization, and water contamination [1,2]. Desalination technology is being studied as an alternative solution to alleviate water resources crisis. Desalination technology can be divided into two categories: (1) The thermal processes including the multi-stage flash evaporation (MSF), multi-effect distillation (MED), and vapor compression (VC); (2) The membrane processes including reverse osmosis (RO) and electrodialysis (ED). In 2013, 65% of the worldwide installed desalination capacity was based on RO, while MSF accounts for 22%, and MED for only 8% [3]. The impetus to install desalination plants in many coastal and metropolitan cities for providing freshwater comes

*Corresponding author.

from the dramatic improvements in energy consumption and reducing investment costs for desalination processes [4].

Membrane distillation (MD) has been known since the 1960s, and developed rapidly in the 1980s with the availability of new membrane material and membrane preparation technology [5]. MD is a thermally driven process, which utilizes water vapor pressure gradient to drive the water vapor across a hydrophobic microporous membrane. Based on different condensation methods, there are mainly four MD configurations: direct contact membrane distillation (DCMD), sweeping gas membrane distillation (SGMD), air gap membrane distillation (AGMD), and vacuum membrane distillation (VMD). In comparison with traditional desalination processes, the advantages of the MD are low operation temperature and pressure, high salt rejection, and low influence of NaCl concentration [5–8]. However, the main challenge for the commercialization of large-scale MD desalination systems is the high energy requirement [9]. In general, the energy consumption in MD systems includes the energy for heating the feed brine and the electricity needed for the pumps and auxiliary devices. Now, many studies are being focused on the design of novel membrane module with energy recovery to decrease the energy consumption. Singh and Sirkar [10] illustrated experimentally AGMD module with internal heat recovery using two sets of hollow fine fibers in one cylindrical module kept in a vertical configuration. And the water vapor flux was up to 25 kg/m^2 h at higher brine inlet temperatures. Cheng et al. [11] designed a novel hollow fiber AGMD module based on the hollow fiber membranes and cooling fibers to improve the permeate flux and to keep the advantage of the high thermal efficiency of AGMD module. Yao et al. [12] developed a continuous-effect membrane distillation (CEMD) process by equipping hollow fiber-based AGMD module which is operated in a countercurrent mode, capable of internal heat recovery.

To achieve the goal of latent heat recovery, appropriate improvement to the MD module is required. In the previous work [12,13], the long length AGMD modules with latent heat recovery using heat exchange hollow fibers were studied including the feed inlet temperature, the feed concentration, and the feed flow rate. And these studies were focused on the overall performance of the AGMD module. But the process of heat and mass transfer needs to be further studied for optimal designing and numerical simulation of AGMD module with energy recovery. In this study, the short length AGMD module with 0.1 m was prepared. The process of heat and mass transfer in AGMD process was studied. The AGMD radial temperature profiles T_h, T_{hm}, T_{pm}, T_{pf}, T_{fc}, T_{cd}, T_c, and the mass transfer coefficients C_m, C_{Km}, C_{Mm}, C_{Ma} were obtained based on the basic transfer equations.

2. Theory

2.1. Mass transfer in AGMD

The heat and mass flows involved in this differential volume of AGMD module are indicated in Fig. 1. The mass transfer in AGMD module includes two processes: the mass transfer across membranes and the mass transfer in the air gap.

The water vapor permeate flux J_D can be expressed as [14,15]:

$$J_m = C_m(P_{hm} - P_{pm}) = \frac{P_{hm} - P_{pm}}{R_m} \quad (1)$$

where C_m is the mass transfer coefficient across membrane, R_m is the mass transfer resistance across membrane. P_{hm} and P_{pm} are the partial pressures of water vapor on both sides of the membrane, respectively.

Mass transfer mechanism in the AGMD process depends on the value of Knudsen number which is defined as the ratio of the mean free path of the water vapor molecule to the pore diameter of the membrane. R_m can be described by molecular diffusion and Knudsen diffusion [12,16,17].

The Knudsen diffusion resistance can be written as [12]:

$$C_{Km} = \frac{1}{R_{Km}} = \frac{\varepsilon d_r}{3\tau\delta_m}\left(\frac{8M_v}{\pi R(T_{avg,m} + 273.15)}\right)^{\frac{1}{2}} \quad (2)$$

And the molecular diffusion resistance is [12]:

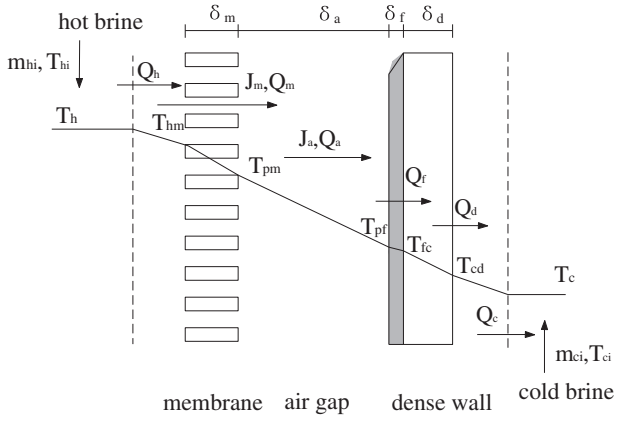

Fig. 1. Heat and mass transfer in AGMD module.

$$C_{Mm} = \frac{1}{R_{Mm}} = \frac{\varepsilon}{\tau\delta_m}\frac{D_{v/a}P_t}{P_{aMa}}\frac{M_v}{R(T_{avg,m}+273.15)} \quad (3)$$

where τ is the membrane tortuosity, ε is the membrane porosity, M_v is the molar mass of water vapor molecule, $T_{avg,m}$ is the mean temperature on both sides of the membrane, P_t is the total pressure of water vapor and air, P_{aMm} is the log-mean air pressure at both sides of the membrane, and $D_{v/a}$ is the diffusion coefficient of the vapor through the air calculated by the Maxwell–Gilliland equation.

In the air gap, R_{Ma} can be described by molecular diffusion because the value of air gap length is much larger than the value of molecular free path of water vapor [11].

$$C_{Ma} = \frac{1}{R_{Ma}} = \frac{1}{\delta_a}\frac{D_{v/a}P_t}{P_{aMa}}\frac{M_v}{R(T_{avg,a}+273.15)} \quad (4)$$

where P_{pm} and P_{pf} are the partial pressures of water vapor within the air gap at T_{pm} and T_{pf}, respectively. $T_{avg,a}$ is the mean temperature within the air gap. P_{aMa} is the log-mean air pressure within the air gap.

The equilibrium vapor pressures P are calculated using the Antoine equation [12].

$$P(T) = 1,000\exp\left(16.262 - \frac{3,799.89}{T+226.35}\right) \quad (5)$$

The presence of sodium chloride influences the equilibrium vapor pressures, Schofield [18] revised $P(T)$ using the method of activity coefficient and P was calculated as:

$$P = x_w\gamma_w P(T) \quad (6)$$

where x_w is the molar concentration of water. γ_w is the activity coefficient of water which is calculated by [19–21].

$$\gamma_w = 1 - 0.5(1-x_w) - 10(1-x_w)^2 \quad (7)$$

2.2. Heat transfer in AGMD

The heat transfer process of AGMD is rather complicated, which includes the heat transfer process within hot feed liquid boundary layer, heat transfer across membrane, heat transfer in air gap, heat transfer in condensation film, heat transfer across hollow fibers, and heat transfer within cold brine liquid boundary layer. Each heat transfer process is expressed as follows [11,12]:

the total heat transfer rate through the hot liquid can be expressed as:

$$Q_h = h_h(T_h - T_{hm})A_h \quad (8)$$

Heat transfer across membrane consists of vapor potential heat Q_L and heat conduction Q_s:

$$Q_m = Q_s + Q_L \quad (9)$$

$$Q_s = \frac{k_m}{r_{im}\ln\frac{d_{om}}{d_{im}}}(T_{hm} - T_{pm})A_m \quad (10)$$

$$Q_L = J_D\Delta H_v A_m \quad (11)$$

where k_m is the thermal conductivity coefficient of membrane and ΔH_v is the evaporation heat of brine, which can be expressed as [11,12]:

$$\Delta H_v = 2.245\times10^3 + 2.475(373.0 - (T+273.15)) \quad (12)$$

The thermal conductivity coefficient of membrane k_m is calculated as:

$$K_m = \varepsilon k_a + (1-\varepsilon)k_s \quad (13)$$

where k_a is the thermal conductivity coefficient of air and k_s is the thermal conductivity coefficient of membrane material.

Heat transfer in air gap:

$$Q_L = J_D\Delta H_v A_m \quad (14)$$

$$Q_s = \frac{k_a}{\delta_a}(T_{pm} - T_{pf})A_a \quad (15)$$

Heat transfer in the water vapor condensed film:

$$Q_f = h_f(T_{pf} - T_{fc})A_f \quad (16)$$

where h_f is the heat transfer coefficient for the condensed film. And h_f can be expressed as [19,22]:

$$h_f = 0.943\left[\frac{k^3\rho^2 g\Delta H_v}{\mu L(T_{pf}-T_{fc})}\right]^{\frac{1}{4}} \quad (17)$$

Heat transfer across heat exchange hollow fibers:

$$Q_d = \frac{k_d}{r_{id}\ln\frac{d_{od}}{d_{id}}}(T_{fc}-T_{cd})A_d \quad (18)$$

Heat transfer in the cold brine boundary:

$$Q_c = h_c(T_{cd}-T_c)A_c \quad (19)$$

The heat transfer coefficients for both hot flow and cold flow can be calculated from the respective local Nusselt number (Nu), which is defined as:

$$Nu_h = \frac{h_h d_{im}}{k_h} \quad (20)$$

$$Nu_c = \frac{h_c d_{id}}{k_c} \quad (21)$$

The maximum R_e is below 1,000 and the flow is laminar. For relative small radial permeation rate, Nu can be estimated as 4.0 [12,23,24], which is an average of $Nu = 3.66$ (for constant wall temperature) and $Nu = 4.36$ (for constant flux).

2.3. Process evaluation

In the process of AGMD desalination, the mass transfer flux J_D is to measure the production capacity of the AGMD module, which can be expressed as:

$$J_D = \frac{m_p}{A_m} \quad (22)$$

The actual driving force of mass transfer in AGMD module is the water vapor pressure difference across the membrane which arises from the temperature difference between T_{hm} and T_{pf}. The temperature difference between T_{hm} and T_{pf} is smaller than the bulk temperature difference between T_h and T_c. The temperature polarization coefficient (TPC) can be introduced to describe temperature polarization phenomenon. TPC is defined as [12]:

$$\mathrm{TPC} = \frac{T_{hm}-T_{pf}}{T_h-T_c} \quad (23)$$

The calculation process of mass transfer resistances R_m, R_{Km}, R_{Mm}, and R_{Ma} were calculated in Eqs. (1)–(4). In the experiment, the operating parameters including the feed inlet temperature (T_{ci}, T_{hi}) and the feed flow rate (m_{ci}, m_{hi}) were set and remained the same. The feed outlet temperature (T_{co}, T_{ho}) and the permeate water flow rate (m_p) were obtained by the experiment. Then the mass transfer flux (J_D) can be calculated according to Eq. (22).

Total heat transfer rate from the hot brine to the cold brine (Q_t) can be expressed as:

$$Q_t = c_p m_{ci}(T_{co}-T_{ci}) \quad (24)$$

In desalination experiment, suitable heat preservation measures were adopted to reduce heat loss as far as possible. In the previous experiments [13,14], the heat loss only occupied 1–2% of the total heat transfer rate from the hot side to the cold side. Now, a short length AGMD module was used and the heat loss can be neglected.

According to the energy conservation, the amount of heat transferred through each of domains is equal to one another at the steady state.

$$Q_h = Q_m = Q_a = Q_f = Q_d = Q_c = Q_t \quad (25)$$

Then, the AGMD radial temperature profiles T_{hm}, T_{pm}, T_{pf}, T_{fc}, T_{cd} and the mass transfer coefficients C_m, C_{Km}, C_{Mm}, C_a were obtained according to Eqs. (1)–(19).

3. Experimental

3.1. Membrane and membrane module

Fig. 2 shows the AGMD module structure. Table 1 shows the characteristics of AGMD modules. The microporous hydrophobic PP hollow fiber membranes and the non-porous heat exchange PP hollow fibers were kindly provided by Tianjin Chemical Separating Technologies Co. Ltd, Tianjin, China. The polypropylene nets were bought, which were placed between each layer of hollow fiber membranes and heat exchange hollow fibers to adjust the width of air gap and to ensure the real existence of air gap.

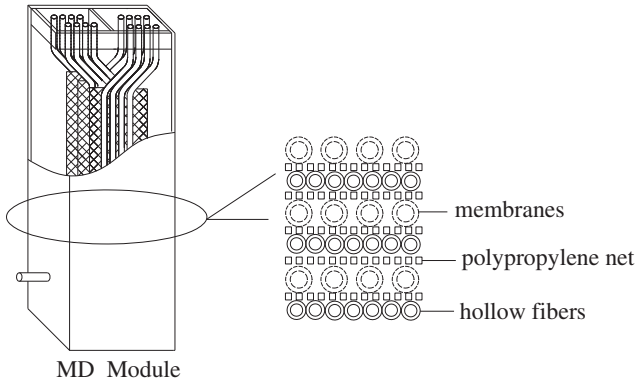

Fig. 2. Schematic presentation of AGMD-HF membrane module.

3.2. Experimental apparatus

The experimental apparatus is schematically depicted in Fig. 3. The AGMD process was operated in a countercurrent flow configuration. The cold brine of 7.0 wt.% NaCl solution in the thermostat A was pumped into the heat exchange hollow fibers. The cold brine temperature was maintained constant at 30˚C (±0.1˚C). In this AGMD module, the cold brine temperature continues to increase as a result of receiving the latent heat of the distillate water vapor from the hollow fiber membranes. To keep the cold brine temperature unchanged or changed little, the large cold brine flow rate (45 L/h) and the small hot brine flow rate (15 L/h) were introduced. As a consequence of that the cold brine changed only slightly in temperature, about 1.5˚C. The hot brine of 7.0 wt.% NaCl solution maintained constant at 70–90˚C (±0.1˚C) was pumped into the inlet of hollow fiber membranes. The temperatures of the feed at four points (two inlets and two outlets) were measured with thermometers Pt100 with sensitivity at 0.1˚C. A good thermal insulation was used to reduce the heat loss. After the whole system was running at steady state, the condensed water collected in a breaker was weighted and then went to the thermostat B to keep the feed concentration unchanged.

4. Results and discussion

4.1. Effect of operating temperature on J_D and TPC

The effects of hot brine inlet temperature (T_{hi}) on the permeate flux (J_D) shown in the Fig. 4 is investigated by varying T_{hi} from 70 to 90˚C with an interval of 5˚C. J_D increases as T_{hi} increases. The driving force of mass transfer in AGMD process increases as T_{hi} increases because of the increase in the trans-membrane vapor pressure difference resulting from the increase in trans-membrane temperature difference. It can be observed that J_D is highly sensitive to the temperature T_{hi}. When T_3 increases from 70 to 90˚C, J_D increases by 244.4% from 4.5 to 15.5 kg/m^2 h. While in Ref. [12], J_D increased by 79% from 3.43 to 6.14 kg/m^2 h in 0.62 m AGMD module, and J_D only increased by 35% when the AGMD module length was increased to 1.07 m. The water vapor pressure increases exponentially with the increase in temperature based on the Antoine equation, which makes the driving force to increase. The measured experimental J_D at different operating conditions is repeatable. The maximum experimental error in J_D is −0.33 kg/m^2 h (3.1%) at T_{hi} = 85˚C, T_{ci} = 30˚C, and F = 15 L/h.

From Fig. 4, J_D of the AGMD module 2 is larger than that of the AGMD module 1. The Knudsen diffusion resistance across membrane (R_{Km}) is much larger than the molecular diffusion resistance across membrane (R_{Mm}) based on the calculation (Eqs. (2) and (3)). R_{Km} is 1,032,227 m^2 Pa s/kg, but R_{Mm} is only 435,649 m^2 Pa s/kg under the operating condition of

Table 1
Characteristics of AGMD modules

Characteristics	AGMD Module	
	Module 1	Module 2
Membrane ID/OD (mm)	0.55/0.7	0.55/0.7
Membrane average pore size (μm)	0.20	0.37
Membrane porosity	69%	68%
Heat exchange hollow fiber ID/OD (mm)	0.4/0.52	0.4/0.52
Number of membranes	100	100
Effective length of module (m)	0.1	0.1
Effective internal membrane area (m^2)	0.017	0.017
Number of heat exchange hollow fibers	200	200
Air gap width (mm)	0.5	0.5

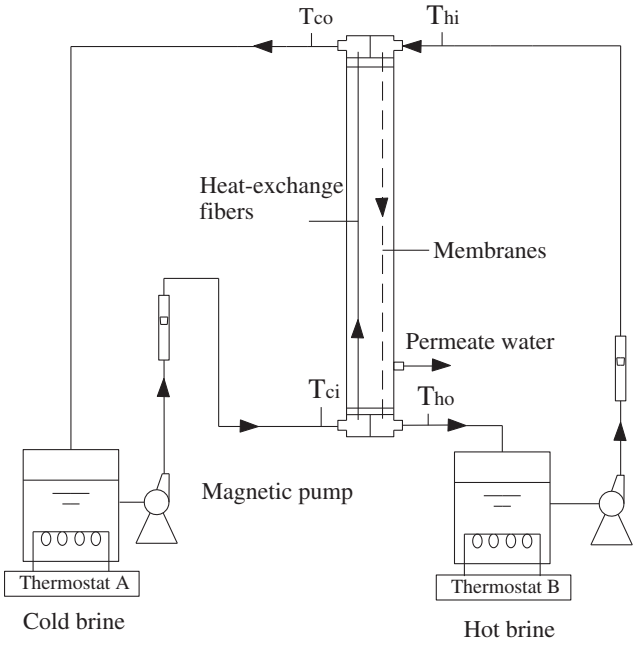

Fig. 3. Schematic diagram of AGMD experimental apparatus.

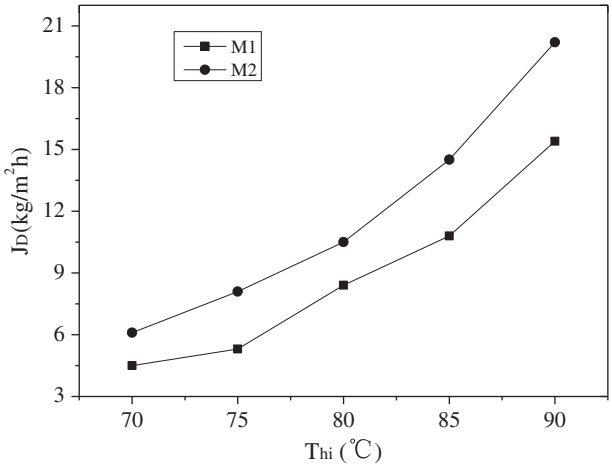

Fig. 4. Effect of hot brine inlet temperature T_{hi} on J_D.

$T_{hi} = 90$℃, $T_{ci} = 30$℃, and $F = 15$ L/h. The mass transfer mechanism across membrane in the ACMD module depends on the value of the mean free path of the water vapor molecule to the pore diameter of the membrane. The Knudsen diffusion resistance dominates the mass transfer process when the membrane pore diameter is small. With the increase in the membrane pore diameter, the domination of Knudsen diffusion weakens, however, the molecular diffusion strengthens, which is beneficial to increase J_D.

Fig. 5 shows that TPC decreases as T_{hi} increases. TPC is proportional to the temperature difference $T_{hm} - T_{pf}$, but it is inversely proportional to the temperature difference $T_h - T_c$ based on Eq. (23). The temperature difference $T_h - T_c$ increases as T_{hi} increases. As shown in Fig. 4, J_D increases with the increase of T_{hi}. The increasing J_D involves more heat flux through the liquid phases, and the temperature gradient in the boundary liquid layers ($T_h - T_{hm}$) increases because the convective heat transfer coefficient of water remains unchanged in the same flow pattern. The heat transfer resistance of across the hollow fibers is primarily controlling when non-porous PP hollow fibers are used as an internal heat exchanger for recovery of latent heat [12]. The temperature difference $T_{fc} - T_{cd}$ also increases with the increase of J_D as shown in the Fig. 6. For this reason, TPC decreases as T_{hi} increases, and J_D does not increase as fast as the water vapor pressure. It is necessary to enhance h_h and h_c for getting a high TPC and J_D, such as by reducing the membrane diameter and the thickness of boundary layer, and meanwhile also to enhance the heat transfer coefficient of the heat exchange hollow fiber, such as by increasing the thermal conductivity of membrane material or further reducing the heat exchange hollow fiber thickness.

4.2. Heat and mass transfer in AGMD module

Table 2 shows the comparison of heat and mass transfer coefficients between modules under the operating condition of $T_{hi} = 90$℃, $T_{ci} = 30$℃, and $F = 15$ L/h. It can be seen that the mass transfer coefficient in air gap (C_{Ma}) is much larger than the mass transfer across the membrane. The mass transfer

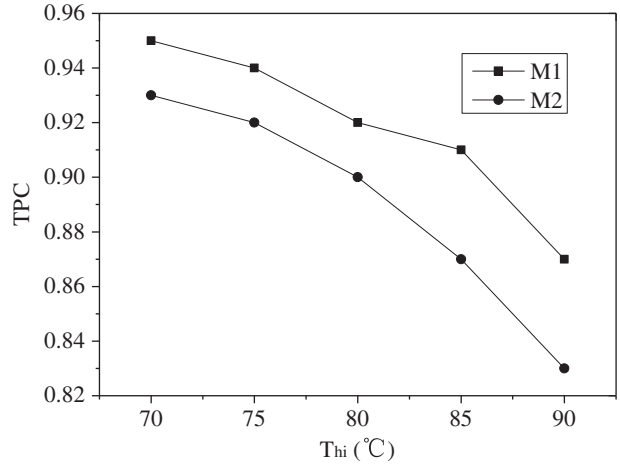

Fig. 5. Effect of hot brine inlet temperature T_{hi} on TPC.

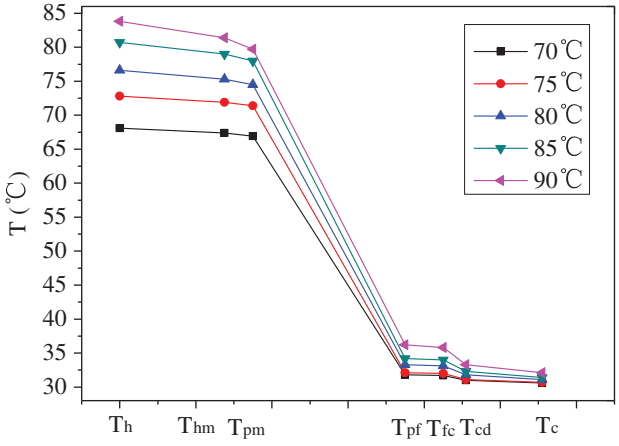

Fig. 6. Temperature profiles of AGMD module 1.

resistance in the air gap (R_{Ma}) occupied the total mass transfer resistance ($R_m + R_{Ma}$) around 30.1% for module 1 and 34.3% for module 2, respectively. Thus, compared with the air gap, the membrane wall is the main resistance for mass transfer. The mass transfer across the membrane is the control procedure. To increase the mass transfer across membrane, it is necessary to enlarge the membrane pore diameter and reduce the membrane thickness. When increasing the membrane pore diameter, it may also affect liquid entry pressure of water (LEPw) and solute rejection. So, when choosing membrane and membrane pore size used in MD desalination experiment, it is necessary to ensure the operating pressure exceeds the LEPw of the membrane based on the Laplace's Law.

The heat transfer coefficient in the boundary layer of hot side (h_h) is about 4,874 W/m^2℃ for module 1 and 5,864.4 W/m^2℃ for module 2. But the heat transfer across the heat exchange hollow fibers is only 3,238.1 W/m^2℃, which indicates that the heat transfer across the heat exchange hollow fiber is the main heat transfer resistance. Based on Eq. (18), the high thermal conductivity of hollow fibers material and thin heat exchange hollow fibers need to be used to increase the heat transfer coefficient across heat exchange hollow fibers.

4.2.1. Temperature profiles of AGMD along the radial direction

Fig. 6 shows the calculated temperature profiles of AGMD along the radial direction according to Eqs. (8)–(19). The temperature drop in the air gap is the highest because the heat transfer coefficient in the air gap is the lowest, which agrees with the reported result in Ref. [12]. The temperature drop in the air gap ($T_{pm} - T_{pf}$) was 43.5℃, which occupied the total temperature drop ($T_h - T_c$) around 84.7% for module 1 under the operating condition of T_{hi} = 90℃, T_{ci} = 30℃, and F = 15 L/h.

The temperature drop across membrane is only about 0.5–1.7℃ in spite of the large total bulk temperature drop. The air gap in AGMD module gives an extra resistance to mass transfer, which makes the permeate flux of AGMD module lower than other MD configurations. However, the heat transfer by heat conduction only occupied the total heat transfer from the hot brine to the cold brine around 5–20% and the value can be up to 20–50% in DCMD module [25]. From the Fig. 6, the temperature drop across the condensed film is only 0.1–0.4℃ because of the high water vapor condensation heat transfer coefficient (14,505.4–14,566.7 W/m^2℃).

4.2.2. Effect of temperature on the mass transfer coefficients (C_{Km}, C_{Mm}, C_m, C_a)

Fig. 7 shows the effect of temperature on the mass transfer coefficients (C_{Km}, C_{Mm}, C_m, C_{Ma}). C_{Km}, C_{Mm},

Table 2
Comparison of heat and mass transfer coefficients between two modules[a]

Heat and transfer coefficients		Module 1	Module 2
Boundary layer of hot side h_h, W/m^2℃		4,874.1	5,864.4
Membrane wall	k_m/r_{im} ln (d_{om}/d_{im}), W/m^2℃	1,079.5	1,109.9
	C_m, 10^{-6} kg/m^2 Pa s	1.35	1.60
	C_{Km}, 10^{-6} kg/m^2 Pa s	0.97	1.73
	C_{Mm}, 10^{-6} kg/m^2 Pa s	3.07	3.01
Air gap	k_a/d_a, W/m^2℃	46	46
	C_{Ma}, 10^{-6} kg/m^2 Pa s	3.11	3.07
Distillate film	h_f, W/m^2℃	14,505.4	14,512.3
Hollow fiber wall	k_d/r_{id} ln (d_{od}/d_{id}), W/m^2℃	3,238.1	3,238.1
Boundary layer of cold side h_c, W/m^2℃		6,137.9	6,146.6

[a]Operating condition: T_{hi} = 90℃, T_{ci} = 30℃, and F = 15 L/h.

C_m, and C_{Ma} decrease with the increase in the temperature. According to Eqs. (2)–(4), the mass transfer coefficients are inversely related to temperature. Compared with the reported relationship between mass transfer coefficient and temperature [12], the calculated values disagree with them because a short AGMD module was used and the bulk temperature was kept unchanged or changed little. The value of C_{Mm} is lower than that of C_{Ma}. It indicates the mass transfer across membrane constitutes the biggest mass transfer resistance because of the large R_{Km}. Based on Eq. (2), C_{Km} can be increased by enlarging the membrane pore diameter and decreasing the membrane thickness.

It can be seen from Fig. 7, the mass transfer coefficient in air gap is the largest when the air gap thickness is kept at a constant value of 0.5 mm. Based on Eq. (4), the mass transfer resistance in the air gap could be the biggest when the air gap thickness was greater than 1.2 mm, which was studied in the Ref.14. Increasing the air gap thickness will decrease the packing density of AGMD module and thus reduces pure water production capacity of per unit area. When the air gap thickness was reduced to 0.2 mm, it could easily form bridges between membranes and heat exchange hollow fibers, and much heat losses by heat conduction were measured because the heat transfer coefficient of liquid is greater than that of the gas. The value of actual mass transfer coefficient across membrane is in close to the value of Knudsen diffusion coefficient across membrane, especially at high hot feed brine temperature.

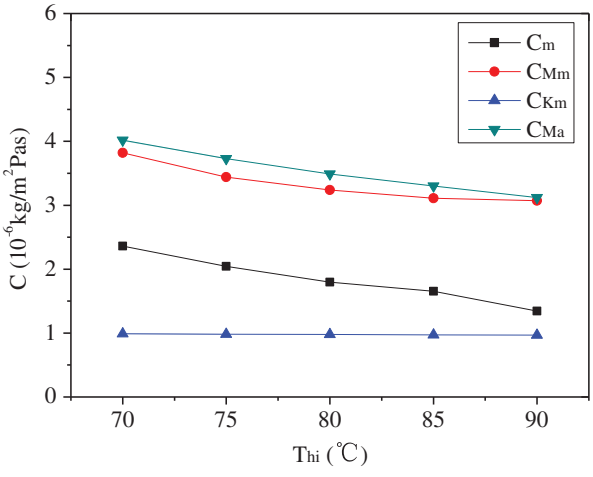

Fig. 7. The effect of temperature on the mass transfer coefficient in AGMD module 1.

5. Conclusions

The heat and mass transfer in AGMD module with internal latent heat recovery was analyzed in details. The AGMD radial temperature profiles T_h, T_{hm}, T_{pm}, T_{pf}, T_{fc}, T_{cd}, T_c, and the mass transfer coefficients C_m, C_{Km}, C_{Mm}, C_{Ma} were obtained.

(1) J_D was highly sensitive to temperature T_{hi}. The maximum value of J_D could reach 15.5 kg/m^2 h at T_{hi} = 90℃ for AGMD module 1. Increasing the membrane pore diameter could increase J_D. For module 2, the membrane pore diameter was 0.37 μm, and J_D could reach 20.2 kg/m^2 h.
(2) C_{Km}, C_{Mm}, C_m, and C_a decreased with the increase in the temperature, T_h. The value of actual mass transfer coefficient across membrane was in close to the value of Knudsen diffusion coefficient across membrane, especially at high T_h. The membrane wall was the main resistance for mass transfer. To increase the mass transfer across membrane, it is necessary to enlarge the membrane pore diameter and reduce the membrane thickness.
(3) The temperature profiles of AGMD along the radial direction (T_h, T_{hm}, T_{pm}, T_{pf}, T_{fc}, T_{cd}, and T_c) were got by establishing the heat and mass transfer model. The temperature drop in the air gap was the highest and occupied the total temperature drop ($T_h - T_c$) around 80–85%.
(4) The heat transfer across the heat exchange hollow fiber was the main heat transfer resistance and the heat transfer across the heat exchange hollow fibers was only around 3,238.1 W/m^2℃. It is necessary to enhance the heat transfer coefficient across the heat exchange hollow fibers such as by reducing the hollow fibers' thickness and the thermal conductivity of hollow fiber material.

Nomenclature

A	—	area, m^2
C_p	—	specific heat, J/kg℃
C	—	mass transfer coefficient, kg/m^{2}Pa s
C_m	—	mass transfer coefficient across membrane, kg/m^{2}Pa s
C_{Mm}	—	molecular diffusion coefficient across membrane, kg/m^{2}Pa s
C_{Km}	—	Knudsen diffusion coefficient across membrane, kg/m^{2}Pa s
C_{Ma}	—	molecular diffusion coefficient in air gap, kg/m^{2}Pa s
d_i	—	inside diameter of the fiber, m

d_o	—	outside diameter of the fiber, m
d_r	—	membrane pore size, m
h	—	convective heat transfer coefficient, $W/m^2/℃$
ΔH_v	—	enthalpy of water evaporation, J/kg
J_D	—	water permeate flux, $kg/m^2/h$
k	—	the thermal conductivity coefficient, W/m℃
P	—	pressure, Pa
R_{Mm}	—	molecular diffusion resistance across membrane, m^2 Pa s/kg
R_{Ma}	—	molecular diffusion resistance in air gap, m^2 Pa s/kg
R_{Km}	—	Knudsen diffusion resistance across membrane, m^2 Pa s/kg
T	—	temperature,℃
ε	—	membrane porosity
μ	—	kinematic viscosity, Pa s
δ	—	thickness, m

Subscripts

a	—	air gap
c	—	cold feed side
d	—	heat exchange hollow fibers
D	—	permeate water
f	—	condensate film
hm	—	hot feed side membrane surface
m	—	hollow fiber membrane
pf	—	distillate film surface
pm	—	membrane surface at air gap side
v	—	vapor

References

[1] S. Miller, H. Shemer, R. Semiat, Energy and environmental issues in desalination, Desalination 366 (2015) 2–8.

[2] V.G. Gude, Energy storage for desalination processes powered by renewable energy and waste heat sources, Appl. Energy 137 (2015) 877–898.

[3] T. Pankratz, IDA Desalination Yearbook, Global Data Report Desalination Data, 2013–2014, Media Analytics Ltc, Oxford, UK, 2014.

[4] A. Stikker, Desal technology can help quench the world's thirst, Water Policy 4 (2002) 47–55.

[5] Y. Yun, R. Ma, W. Zhang, A.G. Fane, J. Li, Direct contact membrane distillation mechanism for high concentration NaCl solutions, Desalination 188 (2006) 251–262.

[6] C.M. Tun, A.G. Fane, J.T. Matheickal, R. Sheikholeslami, Membrane distillation crystallization of concentrated salts-flux and crystal formation, J. Membr. Sci. 257 (2005) 144–155.

[7] X. Li, Y. Qin, R. Liu, K. Yao, Study on concentration of aqueous sulfuric acid solution by multiple-effect membrane distillation, Desalination 307 (2012) 34–41.

[8] U. Dehesa-Carrasco, C.A. Pérez-Rábago, C.A. Arancibia-Bulnes, Experimental evaluation and modeling of internal temperatures in an air gap membrane distillation unit, Desalination 326 (2013) 47–54.

[9] M.S. El-Bourawi, Z. Ding, R. Ma, M. Khayet, A framework for better understanding membrane distillation separation process, J. Membr. Sci. 285 (2006) 4–29.

[10] D. Singh, K.K. Sirkar, Desalination by air gap membrane distillation using a two hollow-fiber-set membrane module, J. Membr. Sci. 421 (2002) 172–179.

[11] L.H. Cheng, P.C. Wu, J. Chen, Numerical simulation and optimal design of AGMD-based hollow fiber modules for desalination, Ind. Eng. Chem. Res. 48 (2009) 4948–4959.

[12] K. Yao, Y. Qin, Y. Yuan, L. Liu, F. He, Y. Wu, A continuous-effect membrane distillation process based on hollow fiber AGMD module with internal latent-heat recovery, AIChE J. 59 (2013) 1278–1297.

[13] H. Geng, H. Wu, P. Li, Q. He, Study on a new air-gap membrane distillation module for desalination, Desalination 334 (2014) 29–38.

[14] H. Geng, Q. He, H. Wu, P. Li, C. Zhang, H. Chang, Experimental study of hollow fiber AGMD modules with energy recovery for high saline water desalination, Desalination 344 (2014) 55–63.

[15] K.W. Lawson, D.R. Lloyd, Membrane distillation, J. Membr. Sci. 124 (1997) 1–25.

[16] M. Qtaishat, T. Matsuura, B. Kruczek, M. Khayet, Heat and mass transfer analysis in direct contact membrane distillation, Desalination 219 (2008) 272–292.

[17] A.M. Alklaibi, N. Lior, Heat and mass transfer resistance analysis of membrane distillation, J. Membr. Sci. 282 (2006) 362–369.

[18] R.W. Schofield, Membrane Distillation, The University of New South Wales, Sydney, 1989.

[19] W.H. McAdams, Heat Transmissions[M], third ed., McGraw-Hill, New York, NY, 1954.

[20] M. Gryta, Concentration of NaCl solution by membrane distillation integrated with crystallization, Sep. Sci. Technol. 37 (2002) 3535–3558.

[21] R.W. Schofield, A.G. Fane, C.J.D. Fell, R. Macoun, Factors affecting flux in membrane distillation, Desalination 77 (1990) 279–294.

[22] C.M. Guijt, I.G. Rácz, J.W. van Heuven, T. Reith, A. de Haan, Modelling of a transmembrane evaporation module for desalination of seawater, Desalination 126 (1999) 119–125.

[23] Y. Qin, J. Cabral, Lumen mass transfer in hollow-fiber membrane processes with constant external resistances, AIChE J. 43 (1997) 1975–1988.

[24] C.M. Guijt, Influence of membrane properties and air gap on the performance of a membrane distillation module, University of Twente, Enschede, The Netherlands, 2003.

[25] A.G. Fane, R.W. Schofield, C.J.D. Fell, The efficient use of energy in membrane distillation, Desalination 64 (1987) 231–243.